nature materials

ARTICLES

PUBLISHED ONLINE: 8 NOVEMBER 2009 | DOI: 10.1038/NMAT2569

Self-assembling chimeric polypeptide–doxorubicin conjugate nanoparticles that abolish tumours after a single injection

J. Andrew MacKay[1]*, Mingnan Chen[2]*, Jonathan R. McDaniel[2], Wenge Liu[2], Andrew J. Simnick[2] and Ashutosh Chilkoti[2]†

New strategies to self-assemble biocompatible materials into nanoscale, drug-loaded packages with improved therapeutic efficacy are needed for nanomedicine. To address this need, we developed artificial recombinant chimeric polypeptides (CPs) that spontaneously self-assemble into sub-100-nm-sized, near-monodisperse nanoparticles on conjugation of diverse hydrophobic molecules, including chemotherapeutics. These CPs consist of a biodegradable polypeptide that is attached to a short Cys-rich segment. Covalent modification of the Cys residues with a structurally diverse set of hydrophobic small molecules, including chemotherapeutics, leads to spontaneous formation of nanoparticles over a range of CP compositions and molecular weights. When used to deliver chemotherapeutics to a murine cancer model, CP nanoparticles have a fourfold higher maximum tolerated dose than free drug, and induce nearly complete tumour regression after a single dose. This simple strategy can promote co-assembly of drugs, imaging agents and targeting moieties into multifunctional nanomedicines.

Packaging clinically approved drugs into nanoscale delivery vehicles (10–100 nm diameter) is of particular interest for cancer therapy, as numerous studies have shown that objects within this size range accumulate within solid tumours owing to the enhanced permeability and retention effect, which results from abnormalities of tumour blood and lymphatic vasculature[1–4]. In our view, drug-loaded nanoparticles for cancer drug delivery should: (1) be easy to synthesize in a few steps with high yield and purity; (2) self-assemble into monodisperse drug-loaded nanoparticles with a size below 100 nm; (3) allow encapsulation of diverse drugs; (4) show favourable pharmacokinetics and tumour accumulation; (5) release the drug with controlled and tunable kinetics; (6) lead to a therapeutic response; and (7) degrade into non-toxic components to enable clearance from the body without adverse toxicity. Although a number of different nanoscale delivery systems have been proposed for cancer therapy[5], most do not satisfy these criteria, which are critical to move these systems into clinical practice.

Motivated by this rationale, we report herein the first example of chimeric polypeptides (CPs) that self-assemble into near-monodisperse, sub-100-nm-sized nanoparticles on drug attachment, and which are biodegradable and show good pharmacokinetics and tumour accumulation, low toxicity and excellent *in vivo* efficacy in a murine tumour model. The CPs consist of two segments, a hydrophilic, biodegradable elastin-like polypeptide (ELP) and a short segment for the attachment of drugs including a cancer chemotherapeutic—doxorubicin (Dox)—through a pH-labile linker (Fig. 1a). ELPs are a class of artificial peptide polymers composed of a Val–Pro–Gly–*Xaa*–Gly repeat derived from human tropoelastin, where the 'guest residue', *Xaa*, can be any mixture of amino acids except proline[6]. We chose ELPs as one of the segments of the CP for multiple reasons. First, ELPs undergo an inverse phase-transition in aqueous solutions at a characteristic transition temperature (T_t), above which they desolvate and phase separate from bulk water[7]. For recombinant ELP block copolymers, this phase-transition behaviour promotes self-assembly into nanostructures, driven by selective desolvation of one block[8–10]. These observations led us to hypothesize that the attachment of multiple copies of a hydrophobic agent, such as Dox or other hydrophobic moieties, would impart sufficient amphiphilicity to the polypeptide to drive its self-assembly into nanoparticles[9,10]. Second, ELPs are useful biopolymers, being non-toxic[11,12], biodegradable and showing good pharmacokinetics[13]. Third, because ELPs can be produced by means of genetic engineering, their composition, molecular weight and polydispersity can be precisely controlled. Fourth, ELPs can be produced with high yield ($\sim$100–200 mg l^{-1}) in *Escherichia coli* and can be easily and rapidly purified by exploiting their phase-transition behaviour[14], so that high-purity, clinical-grade material is easily and cheaply obtained. As one component of the CP system, these attributes of ELPs satisfy many of the proposed requirements for a nanoscale drug carrier.

To ensure favourable pharmacokinetics, the predominant CP described here was engineered to have 160 pentameric repeats where the guest residue *Xaa* = Val/Ala/Gly [1:8:7]. This CP is a hydrophilic polymer (MW = 62.6 kD) with a $T_t \gg 37\,^{\circ}C$ (Supplementary Fig. S1) so that it shows high solubility at body temperature, has a long plasma circulation as seen by its area under the concentration–time curve[13] (AUC) and degrades in serum at the rate of 2.5 wt% day^{-1}. A second, shorter $(Gly–Gly–Cys)_8$ segment was appended at the C-terminal end of the CP to provide drug attachment sites and impart sufficient amphiphilicity to the polymer. This segment provides eight drug attachment points—unique Cys residues—that are clustered at the end of the CP, with embedded diglycine spacers between the attachment sites to minimize steric hindrance during drug conjugation.

[1]Department of Pharmacology and Pharmaceutical Sciences, University of Southern California, Los Angeles, California, 90033-9121, USA, [2]Department of Biomedical Engineering, Duke University, Durham, North Carolina, 27708-0281, USA. *These authors contributed equally to this work.
†e-mail: chilkoti@duke.edu.

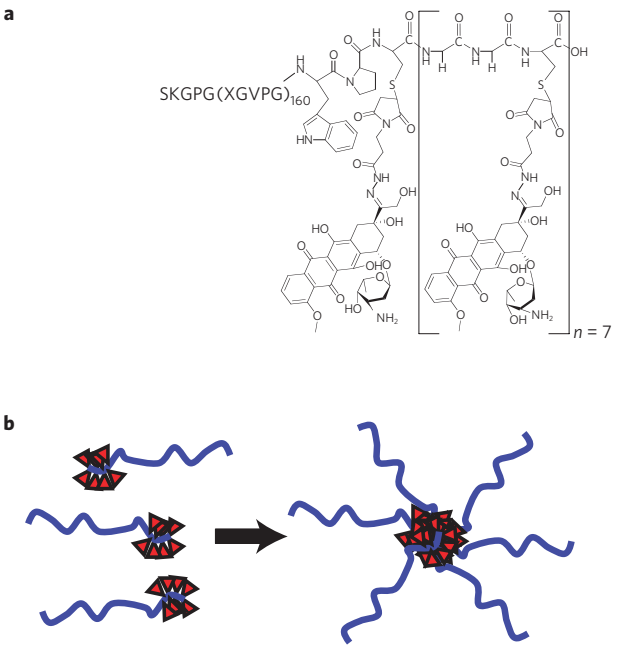

Figure 1 | Structure of CP–Dox conjugate. a, High-molecular-weight ELPs were prepared by genetically encoded biosynthesis and conjugated to Dox at Cys residues by means of a heterobifunctional linker. **b**, The hydrophobic-drug block triggers self-assembly of CP nanoparticles with a drug-rich (red triangles) core surrounded by a hydrophilic polypeptide corona (blue chains).

The CP was over-expressed from a plasmid-borne synthetic gene in *E. coli* using shaker-flask cultures and purified with a yield of $>100\,mg\,l^{-1}$ from the bacterial lysate by inverse transition cycling, a simple, non-chromatographic method[15]. Five rounds of inverse transition cycling provided a monodisperse product with >95% purity, as verified by SDS–polyacrylamide gel electrophoresis (Supplementary Fig. S1) and matrix-assisted laser desorption/ionization mass spectrometry (Supplementary Table S1). To activate Dox for conjugation, it was reacted with *n*-β-maleimidopropionic acid hydrazide tri-fluoroacetic acid to incorporate an internal, acid-labile hydrazone moiety with a terminal maleimide[16,17], and this activated drug was covalently attached to the Cys residues of the CP (Fig. 1a). Purified CP–Dox had 4.8 ± 1.3 (s.d., $n = 3$) drug molecules per polypeptide (Supplementary Table S1).

Results of both transmission electron microscopy (TEM) and dynamic light scattering (DLS) confirmed the spontaneous assembly of CP–Dox into nanoparticles (Fig. 2). Spherical structures of the CP–Dox nanoparticles were observed by freeze-fracture TEM (Fig. 2a) to have a mean particle radius of 19.3 ± 0.9 nm (s.d., $n = 67$; 25th, 50th, 75th percentile = 14, 18, 22 nm). DLS measurements further confirmed the narrow size distribution of CP–Dox nanoparticles with a mean hydrodynamic radius, R_h, of 21.1 ± 1.5 nm (s.d., $n = 11$; 25th, 50th, 75th percentile = 14.3, 16.9, 21.1 nm) (Fig. 2b). In contrast, unmodified CPs have an R_h of 5.5 ± 0.9 nm (s.d., $n = 6$; 25th, 50th, 75th% = 3.9, 4.5, 5.0 nm). DLS results also showed that CP–Dox nanoparticles have a critical aggregation concentration (CAC) below 3 μM CP (14.4 μM Dox Equivalents (Equiv), Supplementary Fig. S1).

The low CAC of the CP–Dox conjugate suggests that it will circulate as self-assembled nanoparticles *in vivo* for an extended period of time. This is because the maximum tolerated dose (MTD) of the CP–Dox nanoparticles in mice is 20 mg Dox Equiv kg^{-1} body weight (BW) (Supplementary Fig. S4), which corresponds to a plasma drug concentration of ~600 μM Dox on injection. The conjugate is hence well above the CAC after intravenous injection. We also observed that the nanoparticles were stable in size and polydispersity at pH 7.4 over a 24 h period, both in the presence and absence of bovine serum albumin (Fig. 2c), indicating that they should exist in systemic circulation as nanoparticles for a significant period of time. Furthermore, the ~40 nm diameter of these nanoparticles is below the pore size of the permeable vasculature found in many solid tumours, suggesting that CP–Dox nanoparticles should be able to selectively accumulate in a solid tumour by means of the enhanced permeability and retention effect[1,3,4]. In contrast, at pH 5.0, the polydispersity of CP–Dox nanoparticles increased with time, which is suggestive of the release of Dox from the CP–Dox conjugate by means of acid-catalysed cleavage of the hydrazone bonds, and subsequent disassembly of the nanoparticles (Fig. 2c).

The formation of nanoparticles is not restricted to the conjugation of multiple copies of Dox to the CP. It is notable that the attachment of five structurally diverse small molecules (Supplementary Fig. S2) to CPs also triggered their spontaneous self-assembly into near-monodisperse nanoparticles with a size range ($R_h = 11.2$–41.7 nm) (Supplementary Table S2). Furthermore, this behaviour is not restricted to a single CP, and five different CPs with a range of molecular weights and compositions also self-assemble into nanoparticles on conjugation to Dox (Supplementary Table S2). The self-assembly of nanoparticles on conjugation of multiple copies of diverse hydrophobic small molecules suggests that the attachment-triggered self-assembly of CPs is potentially a robust and general principle for the formation of nanoparticles with a core that sequesters hydrophobic drugs and a corona comprising hydrophilic polypeptide chains (Fig. 1b).

The liberation of free drug from the CP–Dox nanoparticles requires the pH-dependent cleavage of the hydrazone bond (Fig. 1a). To verify the kinetics of drug release, CP–Dox nanoparticles were incubated either at pH 7.4 or pH 5.0 at 37 °C for 24 h (Fig. 2d). The release of free drug was monitored by size-exclusion high-performance liquid chromatography (HPLC). At pH 7.4, the hydrazone bond was stable, and no significant release of free drug was observed over 24 h. In contrast, at pH 5.0, free drug was generated with a first-order half-life of 4.9 ± 0.5 h (confidence interval (CI) 95%) and reached a maximum release of 68 ± 3% (CI 95%) of the initial amount of Dox (Supplementary Table S1), similar to the levels observed with other polymeric hydrazones[18]. These data confirm that the covalent bond to Dox is exceptionally stable at the pH of blood, but that the bond cleaves at an appreciable rate at a pH that is relevant to endo–lysosomal trafficking. As CP–Dox conjugates have previously been demonstrated to localize within low-pH compartments in cellular uptake assays[19], the pH-dependent release of Dox from the CP–Dox conjugate suggests endo–lysosomal release of the drug following cellular uptake of the CP–Dox nanoparticles.

To explore the mechanism of CP–Dox internalization and intracellular drug delivery, cells were observed by laser-scanning confocal fluorescence microscopy at various time points after incubation with free Dox (Fig. 3a–c), free CP (Fig. 3d–f) and CP–Dox (Fig. 3g–i). Free Dox rapidly accumulated in the nucleus after incubation for 5 min (Fig. 3a). To observe the cellular fate of free CP, the polypeptide was labelled with Oregon Green by means of a pH-insensitive thio-ether bond (Supplementary Table S2). CP–Oregon Green led to intense punctate fluorescence in the cytoplasm after 30 min (Fig. 3e), suggesting the localization of the CP to endosomes and lysosomes. In contrast, Dox delivered by means of CP nanoparticles showed intermediate behaviour between free Dox and free CP. There was very low accumulation of Dox in the nucleus at 5 min following incubation with CP–Dox, indicative of the slower uptake of CP–Dox compared with free Dox; however, there was significant accumulation of Dox within the nucleus 30 min after incubation with CP–Dox (Fig. 3h). These results suggest that Dox accumulation in the nucleus after incubation

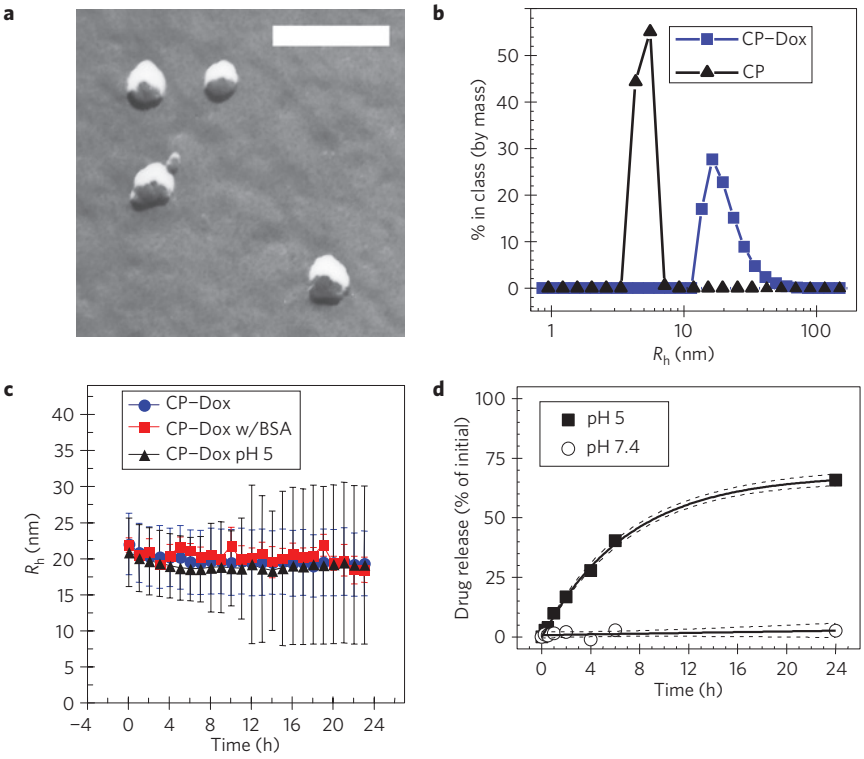

Figure 2 | Characterization of CP–Dox nanoparticles. a, Freeze-fracture TEM image of CP–Dox nanoparticles (scale bar: 200 nm). **b**, Distribution of hydrodynamic radii for CP and CP–Dox nanoparticles at 25 μM in PBS at 37 °C by DLS. **c**, CP–Dox nanoparticles have a stable hydrodynamic radius over time in PBS at pH 7.4, PBS with 0.1 mM bovine serum albumin (BSA) and in buffer at pH 5.0; however, the distribution of hydrodynamic radii (error bars) increases over time at low pH (mean ± s.d.). **d**, The kinetics of particle-diameter broadening are in agreement with the pH-dependent release of Dox from CP–Dox nanoparticles as determined using size-exclusion chromatography at pH 7.4 and 5.0. The fit line (solid) and 95% confidence interval lines (dashed) are shown.

of cells with CP–Dox is a result of cellular uptake of CP–Dox nanoparticles, intracellular drug release and subsequent trafficking of drug to the nucleus.

To evaluate the behaviour of CP–Dox nanoparticles in mice, the conjugates were administered systemically and the plasma drug concentration was measured as a function of time post-injection. The data were fitted to a two-compartment pharmacokinetic model (Supplementary Information), yielding a terminal half-life of 9.3 ± 2.1 h (95% CI) and a plasma AUC of 716 ± 139 μM h (95% CI) (Fig. 4a, Supplementary Table S3). The AUC for a mouse treated with the same dose of free Dox is only 4.7 μM h (ref. 20). On the basis of this significant increase in plasma AUC, these results suggested that CP–Dox nanoparticles are likely to preferentially accumulate in solid tumours as compared with free drug.

Motivated by these findings, we next evaluated tissue exposure to Dox. Mice were administered free drug or CP–Dox nanoparticles, and tissue samples were obtained after 2 or 24 h (Fig. 4b,c). Notably, 24 h after administration of CP–Dox, the tumour had a significant 3.5-fold increase in drug concentration as compared with free drug at the same dose (Fig. 4b; Tukey's Honestly Significant Difference (HSD); $p = 2 \times 10^{-6}$). Equally important, the CP–Dox nanoparticles significantly reduced the drug concentration at several non-tumour sites in the body, including the muscle, the lung (Supplementary Fig. S4) and the heart (Fig. 4c). In particular, the incorporation of Dox into CP nanoparticles decreased the peak concentration in the heart by 2.6-fold compared with free Dox (Tukey's HSD; $p = 1 \times 10^{-6}$). The decreased accumulation in the heart is notable, as cardiomyopathy is the dose-limiting side effect of free Dox (ref. 21). The increase in tumour exposure and decrease in heart exposure is one mechanism that explains why the MTD of CP–Dox nanoparticles is higher than that of free Dox (Supplementary Fig. S4, Table S4), and suggested that CP–Dox encapsulation may improve the therapeutic index of Dox.

To compare the therapeutic effect of free Dox and CP–Dox nanoparticles, both formulations were administered in a dose escalation study to determine their MTD. The MTD of Dox was 5 mg kg^{-1} BW and the MTD for CP–Dox was 20 mg Dox Equiv kg^{-1} BW (Supplementary Fig. S4). Thus, by administration of the MTD of CP–Dox nanoparticles, which is fourfold greater than the MTD of free drug, it is potentially possible to increase the absolute concentration of drug in the tumour at 24 h by an estimated $4 \times 3.5 = 14$-fold over free drug.

CP–Dox nanoparticles were next evaluated for their anti-tumour activity at their MTD. Mice with eight-day-old C26 tumours (25th, 50th, 75th percentile = 17, 21, 66 mm^3 tumour volume) were treated with PBS, Dox or CP–Dox nanoparticles (Fig. 5a). Fifteen days after tumour implantation, CP–Dox-treated mice had a mean tumour volume of 13 mm^3 ($n = 9$) versus 329 mm^3 ($n = 10$) for PBS- (Mann–Whitney; $p = 0.00{,}002$) and versus 166 mm^3 ($n = 10$) for free-drug- (Mann–Whitney; $p = 0.03$) treated controls. Clearly, the CP–Dox formulation at the MTD outperforms free drug in reducing tumour volume, which correlated with a substantial increase in animal survival (Fig. 5b). The median survival time for mice treated with PBS ($n = 10$) was 21 days, and treatment with Dox ($n = 10$) slightly increased this survival to 27 days (Kaplan–Meier, $p = 0.03$). In contrast, the CP–Dox nanoparticles cured eight of nine mice for up to 66 days after tumour implantation, a significant improvement over free drug (Kaplan–Meier, $p = 0.0002$). Thus, with only a single dose injection, CP–Dox nanoparticles provide a substantial curative effect.

To explore the mechanism by which CP–Dox nanoparticles outperform the free drug, we next compared the genomic profiles

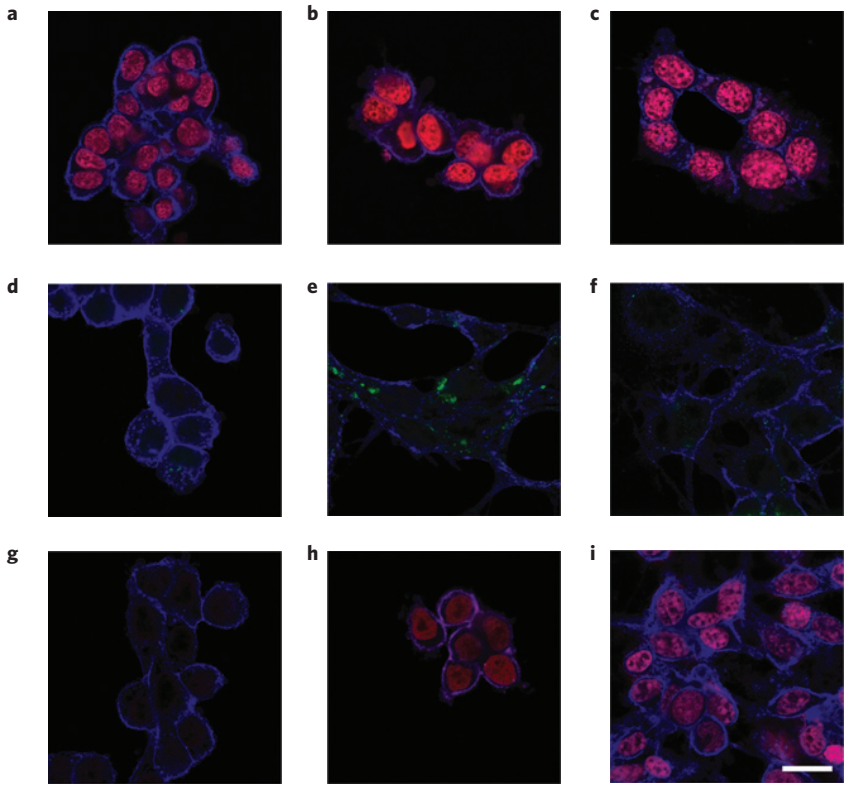

Figure 3 | Internalization of CP–Dox and delivery of drug to the nucleus. a–i, Laser-scanning confocal microscopy images of C26 cells (blue) that show cellular uptake for free Dox (**a**–**c**), CP–Oregon Green (**d**–**f**) and CP–Dox (**g**–**i**) at 5 min (**a**,**d**,**g**), 30 min (**b**,**e**,**h**) and 24 h (**c**,**f**,**i**). Free Dox (red) rapidly localizes to the nucleus at all time points. CP–Oregon Green (green) is internalized into the cytoplasm with punctate staining after 30 min. CP–Dox (red) nanoparticles produce intense nuclear staining with drug after 30 min (scale bar: 20 μm).

for tumours obtained from mice administered with PBS, free Dox or CP–Dox, two days after treatment. The comparison between CP–Dox and PBS produced many differences, and the detailed analysis of these results exceeds the scope of this article and will be reported elsewhere. Instead, we focused on comparison of the gene-array data between CP–Dox and free Dox to elucidate any potential differences in the molecular mechanism(s) of tumour cell death elicited by the CP–Dox nanoparticles. We identified 14 genes that differed significantly ($p < 0.00012$) between CP–Dox and free Dox given at the MTD (Fig. 6a). A hierarchical clustering analysis (Fig. 6b) was carried out whereby genes were linked together according to their expression patterns (dendrogram on left) and individual mice were clustered (dendrogram on top). For all mice, the clustering results matched their treatment, suggesting that these genes may be useful biomarkers to indicate tumour responses to CP nanoparticles (Fig. 6b).

Unlike either free Dox or PBS, the CP–Dox formulation upregulated programmed cell death and negative regulators of the cell cycle (Supplementary Table S5). A primary mechanism of Dox cytotoxicity is mediated by topoisomerase-II, which cleaves genomic DNA, allows adjacent DNA strands to crossover, relieving rotational strain, and permits the successful repair of breakages. Dox intercalates with DNA and freezes topoisomerase-II to the ends of freshly cut DNA, which leads to permanent DNA damage and exit from the cell cycle[22]. Although numerous genes are involved in DNA repair[23], this analysis identified one particular gene, uracil-DNA glycosylase (*Ung*), that is downregulated only by CP–Dox treatment (Fig. 6b); furthermore, *Ung* is associated with resistance to chemotherapeutics, including Dox[24,25]. By downregulating DNA repair, CP–Dox may directly enhance the anti-tumour drug effect. These data provide mechanistic insights into CP nanoparticle delivery and support the contention that CP nanoparticles may overcome drug resistance, as has been suggested for other drug-delivery systems[26–28].

The closest analogue to the present system are monoblock poly(ethylene glycol) (PEG)–Dox conjugates that seem to form micelles, but their self-assembly was explored with only a single hydrophobic drug (Dox), so it remains unclear whether this approach will apply to other hydrophobic drugs and polymers[29]. Furthermore, in comparison with CP–Dox, the PEG–Dox conjugate showed limited efficacy in extending the survival time and did not produce long-term cures in an animal model. Other methods to create drug-loaded polymer nanoparticles have relied on: (1) the chemical synthesis of amphiphilic PEG-based biohybrid block copolymers to encapsulate the drug[18,30–32]; (2) the synthesis of complex terpolymers in which the copolymerization or attachment of fatty acids or cholesterol to the polymer chain drives its self-assembly[33,34]; or (3) the design of sophisticated and complex dendrimer architectures[3]. Although all of these approaches have their merits, they are far more complicated than the genetically encoded delivery system described herein, as they rely on complex, multistep synthesis of polymers, which can be difficult to scale up. Many synthetic polymeric vehicles are not degradable, nor have they been shown to self-assemble across a broad range of hydrophobic molecules. A high degree of pharmaceutical complexity typifies many methods of nano-encapsulation. For example, methods that rely on physical encapsulation and size fractionation of nanoparticles, such as polymer micelles[3], liposomes[1] and emulsion polymerization[35], are highly multicomponent systems (that is, drugs, buffers, mixtures of amphiphiles, monomers, solvents and excipients), which can hinder pharmaceutical viability.

In contrast, the CP nanoparticle system is, we believe, the first example of a simple and rationally designed recombinant polypeptide that is extraordinarily efficient to synthesize and

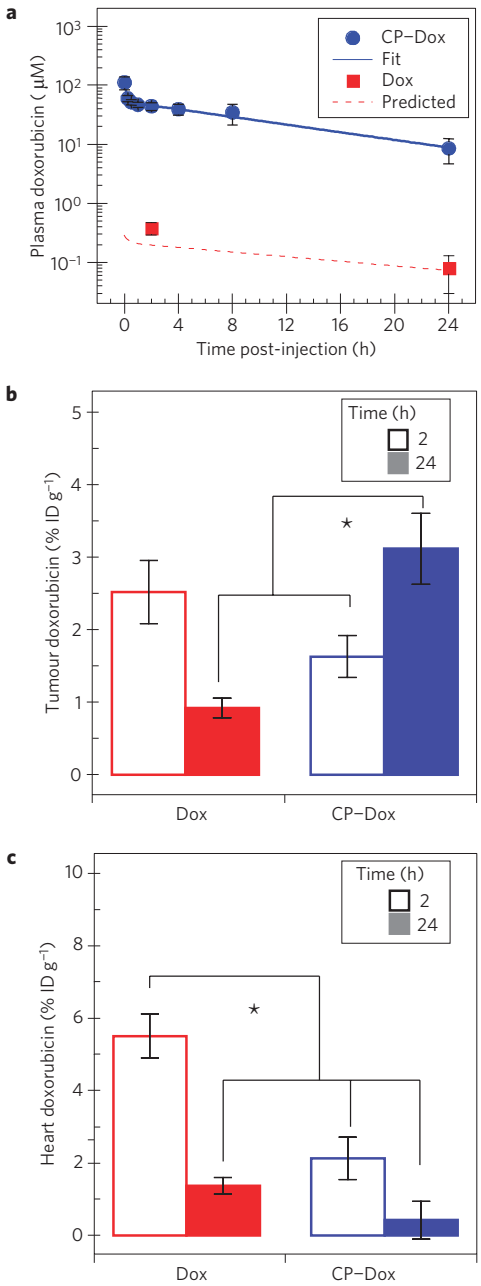

Figure 4 | Plasma pharmacokinetics and tissue biodistribution. a, Plasma Dox concentrations as a function of time post-injection. A two-compartment model was fitted to the plasma Dox concentration, which yielded a terminal half-life of 9.3 ± 2.1 h (CI 95%) for CP-Dox. The concentration of free Dox has been confirmed at two time points experimentally; furthermore, the observed concentrations correlate with the prediction of a pharmacokinetic model of free Dox in mice[20] (Supplementary Table S3) (mean ± 95% CI; $n = 5$–8). **b**,**c**, The Dox concentration in tumour tissue (**b**) and heart tissue (**c**) at 2 and 24 h post-administration. * indicates $p < 0.0005$ (analysis of variance, Tukey's HSD) (mean ± s.d.; $n = 4$–6).

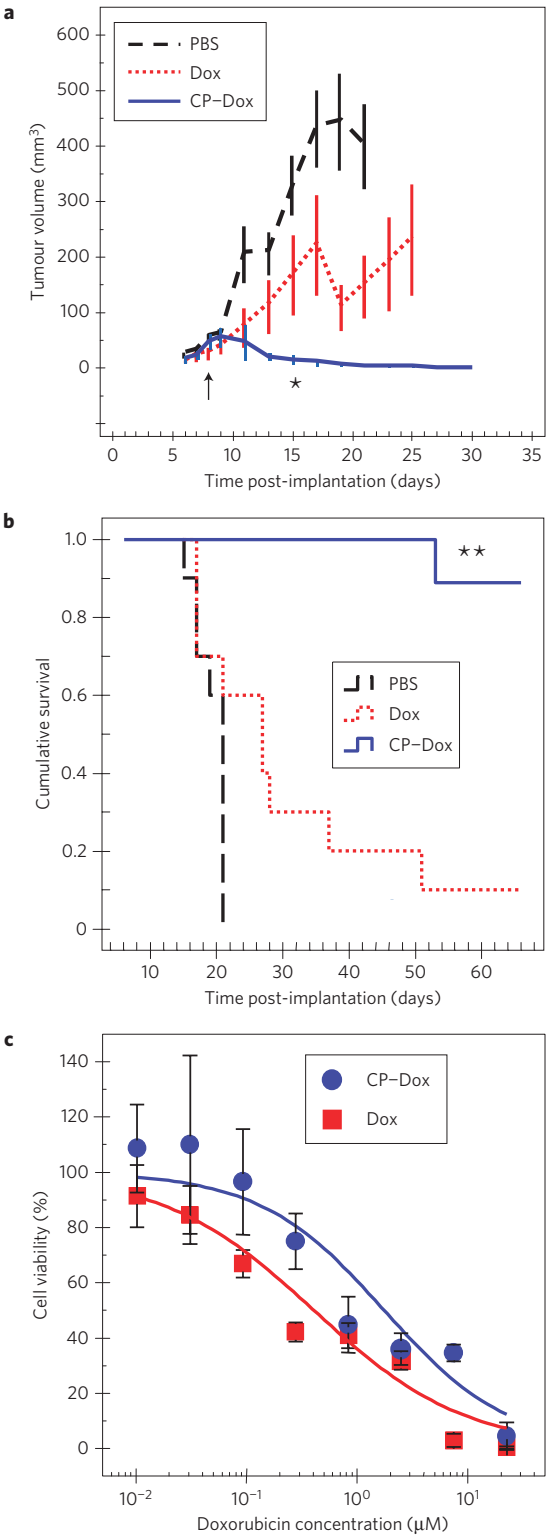

Figure 5 | Anti-tumour activity of CP-Dox nanoparticles. For **a**,**b**, tumour cells (C26) were implanted subcutaneously on day zero. Mice were treated on day 8 (↑) at the MTD with PBS ($n = 10$), free Dox (5 mg kg^{-1} BW; $n = 10$) and CP-Dox (20 mg Dox Equiv kg^{-1}BW; $n = 9$). **a**, Tumour volume up to day 30 (mean ± s.d.; $n = 6$–10). * indicates $p = 0.03$, 0.00002 for CP-Dox versus Dox and PBS (day 15) respectively (Mann–Whitney). **b**, Cumulative survival of mice. ** indicates $p = 0.0001$, 0.00004 for CP-Dox versus Dox and PBS respectively (Kaplan–Meier). **c**, Cell viability for CP-Dox ($n = 4$; $IC_{50} = 1.8$ μM) and free Dox ($n = 14$; $IC_{50} = 0.41$ μM) in C26 cells. (Mean ± 95% CI.)

purify from *E. coli* and self-assembles into nearly monodisperse sub-100-nm nanoparticles in water, thereby obviating the need for organic solvents during processing. This attachment-triggered self-assembly of CPs is conserved across a range of small hydrophobic molecules, which further distinguishes it from previous studies with synthetic polymers that are restricted to one or a few hydrophobic molecules (Supplementary Table S2). In addition, the degree of

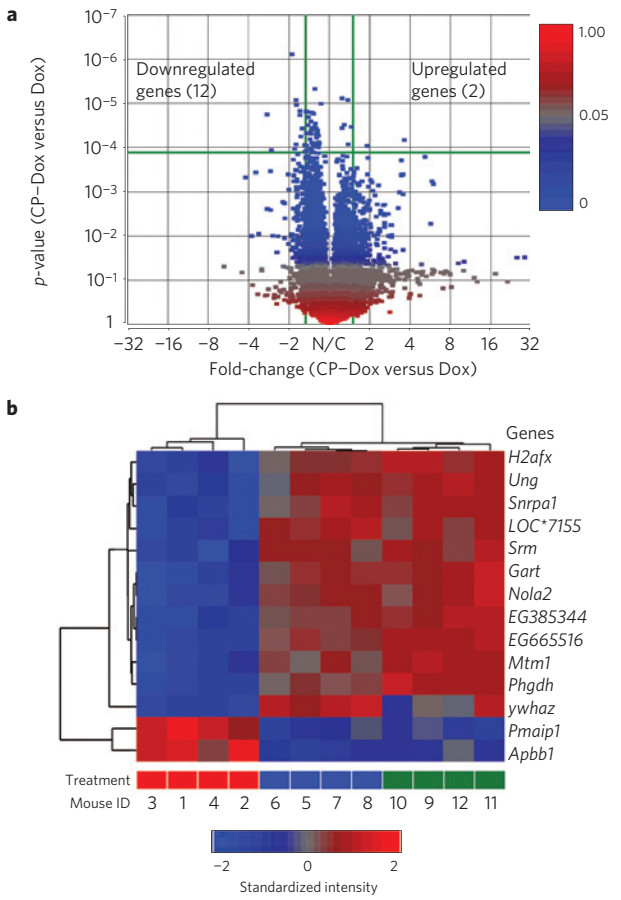

Figure 6 | Genomic profiles of CP–Dox- and free-Dox-treated tumour tissues. a, Volcano plot of gene expression contrasting CP–Dox-treated mice versus Dox-treated mice. The expression level is denoted by a square coloured to reflect the *p*-value. The horizontal green line indicates the cutoff of the *p*-value ($p < 0.00012$), which corrects for multiple comparisons. The vertical green lines indicate the cutoff for a significant fold change (>1.5-fold). In CP–Dox-treated mice, 12 genes were significantly downregulated and two genes were upregulated in contrast to Dox-treated mice. **b**, A hierarchical clustering analysis was carried out on the basis of the expression pattern. The genes were linked together according to their expression (dendrogram on left). Individual mice were also clustered (dendrogram on top). For all mice, the clustering results match their treatment: CP–Dox (red bar); Dox (blue bar); PBS (green bar). The gene-expression intensities were standardized between −2.0 (blue) and 2.0 (red). *LOC*7155* is an abbreviation of an untitled gene *LOC100047155*.

drug loading and particle diameter are conveniently controlled at the design level by the number of unique reactive sites that are appended to chain termini of a CP and its molecular weight, orthogonal variables that are precisely and trivially encoded into the gene-level design of the polymer. Furthermore, attachment of drug solely at the chain end ensures that the drug is sequestered in the nanoparticle core—unlike other nanoparticle drug carriers, such as dendrimers[3], metal nanoparticles[36] or carbon nanotubes[37]. The ability to deterministically place the drug molecules at the end of the polymer chain also differentiates this system from many protein and polymer conjugates where the reactive sites are distributed along the polymer chain or protein surface. Such arrangements leave the drug exposed to the solution environment and do not necessarily impart amphiphilic self-assembly of a nanostructures[2,3,38]. In common with other peptide–drug conjugates[2], our approach permits control over release (rate, mechanism, *in vivo* location) through the design of linker chemistry. For example, the linker described here contains an internal, acid-labile hydrazone bond[3,16,17] that triggers intracellular drug release in endosomes and lysosomes. Similarly, peptide linkers that are substrates for tumour-specific proteases (cathepsins and matrix metalloproteases) may enable preferential release in the tumour[2,39]. Both approaches can be easily incorporated into a CP by means of recombinant DNA methodology.

The genetically engineered CP nanoparticles described herein, hence present four important points of novelty: (1) generality: the assembly of these polypeptides into near-monodisperse nanoparticles is conserved across a range of small molecules and polypeptides (Supplementary Table S2); (2) genetically encoded synthesis: the use of recombinant DNA methodology provides a trivial mechanism for controlling particle diameter, degree of drug loading and incorporation of other biologically active peptides; (3) simplicity, as these self-assembling subunits result from a simple two-step synthesis consisting of polypeptide biosynthesis followed by covalent drug conjugation; and (4) biodegradability, as these polypeptides may be used at molecular weights above the renal filtration cutoff, beyond which non-biodegradable polymers undergo chronic accumulation. We believe that this combination of features makes the CP formulation uniquely attractive for the development of advanced nanoparticle drug carriers.

Methods

CPs were synthesized by heterologous expression of a plasmid-borne synthetic gene in *E. coli* as described previously[14]. Dox (MW = 580 g mol^{-1}) was covalently linked to cysteine residues on CPs (Supplementary Information). The molar extinction coefficient for Dox was determined in PBS at 495 nm ($\varepsilon = 1.00 \times 10^4$ M^{-1} cm^{-1}) and used to determine drug concentration.

DLS was used to measure the particle radius at 37 °C after filtration through an Anotop syringe filter with 0.1 μm size pores (Whatman) using a DynaPro Plate Reader (Wyatt Technology). Freeze-fracture TEM was also used to estimate particle radius on a JEOL 100 CX electron microscope (Nano Analytical Laboratory). The radii for particles were analysed using ImageJ 1.34i (NIH) using the measurement tool.

HPLC was used to determine the fraction of drug remaining bound using an LC10 HPLC (Shimadzu Scientific Instruments) and a Shodex OHPak KB-804 column. To assay for the release of drug, samples of CP–Dox in PBS (10 mM NaH_2PO_4, 140 mM NaCl, pH 7.4) were diluted into either pH 5.0 (0.1 M Na acetate) or pH 7.4 (0.1 M NaH_2PO_4). Samples were incubated at 37 °C, quenched at pH 7.4 and measured for free Dox at 14.7 min (CP–Dox eluted at 8.8 min). The percentage of drug released, $F_{\%,\text{released}}$, was fitted to a first-order model:

$$F_{\%,\text{released}} = a\left[1 - e^{\left(\frac{-\ln(2)t}{t_{1/2}}\right)}\right]$$

where t is the time after incubation, $t_{1/2}$ is the half-life of release and a is the maximum cleavage.

A murine colon carcinoma cell line, C26, was used to evaluate the potency of Dox both *in vitro* and *in vivo*. *In vitro* cytotoxicity was determined in a 96-well format, where cells were incubated for 1 day before addition of drug. Blank wells and PBS-treated wells were defined as 0 and 100% viability. Dilutions of drug were incubated with cells for 3 days. CellTiter 96 AQueous (Promega) reagent (20 μl) was added to each well (120 μl total) and incubated before measurement. The 50% inhibitory concentration, IC_{50}, was determined by fitting to the following equation:

$$V_{\%} = 100\% \Big/ \left[1 + \left(\frac{C_{\text{Dox}}}{IC_{50}}\right)^{p}\right]$$

where $V_{\%}$ is the viability, C_{Dox} is the Dox concentration and p defines the slope of the curve.

To study cellular uptake, cells were seeded in 8-well Lab-Tek II chamber slides (Thermo Fisher Scientific) at the density of 8×10^4 cells per chamber and allowed to attach overnight. Cells were then treated with free Dox, CP–Oregon Green or CP–Dox at the concentration of 40 μM Equiv of Dox or Oregon Green at 37 °C for different time periods. After treatment, the cells were washed with Dulbecco's PBS, fixed in 2% paraformaldehyde, stained with Alexa Fluor 594 wheat germ agglutinin (W11262; Invitrogen), washed with Dulbecco's PBS five times and imaged using an LSM5 upright laser-scanning confocal microscope (Zeiss) with a ×100 oil-immersion objective. The following wavelengths were used: excitation at 545 nm and detection through a 595 nm high-pass filter for W11262, excitation at 488 nm and detection through a 505–550 nm band-pass

filter for Oregon Green and excitation at 488 nm and detection through a 560 nm low-pass filter for Dox.

To evaluate the *in vivo* activity of CP–Dox, animals were treated in accordance with National Institute of Health Guide for the Care and Use of Laboratory Animals as approved by the Duke University Institutional Animal Care and Use Committee. A BALB/c mouse tumour model was developed by subcutaneous injection of $2.5–5 \times 10^5$ cells giving >95% tumour-take. For the pharmacokinetic study, CP–Dox was administered systemically (5 mg Dox Equiv kg^{-1} BW) and sampled through the tail vein, and the plasma concentration of CP–Dox was fitted to a two-compartment pharmacokinetic model using SAAMII (University of Washington, Seattle, Washington). For the biodistribution study, the drug was administered systemically 8 days after implantation. At 2 and 24 h post-administration, tissue samples were assayed for drug concentration using calibrated fluorometry (Supplementary Information). Biodistribution data were compared using analysis of variance followed by Tukey's HSD test. In studies of therapeutic efficacy, mice (6–8 weeks old) bearing dorsal tumours were treated 8 days after implantation. Tumour dimensions and body weight were determined 3–4 times a week, and the tumour volume was calculated:

$$\text{Volume} = \text{length} \times \text{width}^2 \times \pi/6$$

Mice showing more than 15% BW loss or tumours greater than 1,000 mm^3 were euthanized. Tumour volumes were compared using a Kruskal–Wallis test followed by a Mann–Whitney test. Cumulative survival curves were compared using Kaplan–Meier analysis followed by the Log Rank Test. Statistics were calculated using SPSS 15.0.

Received 13 April 2009; accepted 2 October 2009; published online 8 November 2009

References

1. Drummond, D. C., Meyer, O., Hong, K., Kirpotin, D. B. & Papahadjopoulos, D. Optimizing liposomes for delivery of chemotherapeutic agents to solid tumors. *Pharmacol. Rev.* **51,** 691–743 (1999).
2. Duncan, R. Polymer conjugates as anticancer nanomedicines. *Nature Rev. Cancer* **6,** 688–701 (2006).
3. Lee, C. C., MacKay, J. A., Frechet, J. M. & Szoka, F. C. Designing dendrimers for biological applications. *Nature Biotechnol.* **23,** 1517–1526 (2005).
4. Matsumura, Y. & Maeda, H. A new concept for macromolecular therapeutics in cancer chemotherapy: Mechanism of tumoritropic accumulation of proteins and the antitumor agent smancs. *Cancer Res.* **46,** 6387–6392 (1986).
5. Brannon-Peppas, L. & Blanchette, J. O. Nanoparticle and targeted systems for cancer therapy. *Adv. Drug Deliv. Rev.* **56,** 1649–1659 (2004).
6. Urry, D. W. Physical chemistry of biological free energy transduction as demonstrated by elastic protein-based polymers. *J. Phys. Chem. B* **101,** 11007–11028 (1997).
7. Yamaoka, T. *et al.* Mechanism for the phase transition of a genetically engineered elastin model peptide (VPGIG)(40) in aqueous solution. *Biomacromolecules* **4,** 1680–1685 (2003).
8. Cappello, J. *et al. In situ* self-assembling protein polymer gel systems for administration, delivery, and release of drugs. *J. Control. Release* **53,** 105–117 (1998).
9. Dreher, M. R. *et al.* Temperature triggered self-assembly of polypeptides into multivalent spherical micelles. *J. Am. Chem. Soc.* **130,** 687–694 (2008).
10. Wright, E. R. & Conticello, V. P. Self-assembly of block copolymers derived from elastin-mimetic polypeptide sequences. *Adv. Drug Deliv. Rev.* **54,** 1057–1073 (2002).
11. Megeed, Z., Cappello, J. & Ghandehari, H. Genetically engineered silk-elastinlike protein polymers for controlled drug delivery. *Adv. Drug Deliv. Rev.* **54,** 1075–1091 (2002).
12. Urry, D. W., Parker, T. M., Reid, M. C. & Gowda, D. C. Biocompatibility of the bioelastic materials, poly(Gvgvp) and its gamma-irradiation cross-linked matrix—summary of generic biological test-results. *J. Bioact. Compat. Polym.* **6,** 263–282 (1991).
13. Liu, W. *et al.* Tumor accumulation, degradation and pharmacokinetics of elastin-like polypeptides in nude mice. *J. Control. Release* **116,** 170–178 (2006).
14. Chilkoti, A., Dreher, M. R. & Meyer, D. E. Design of thermally responsive, recombinant polypeptide carriers for targeted drug delivery. *Adv. Drug Deliv. Rev.* **54,** 1093–1111 (2002).
15. Meyer, D. E. & Chilkoti, A. Purification of recombinant proteins by fusion with thermally-responsive polypeptides. *Nature Biotechnol.* **17,** 1112–1115 (1999).
16. Furgeson, D. Y., Dreher, M. R. & Chilkoti, A. Structural optimization of a 'smart' doxorubicin–polypeptide conjugate for thermally targeted delivery to solid tumors. *J. Control. Release* **110,** 362–369 (2006).
17. Rodrigues, P. C. *et al.* Acid-sensitive polyethylene glycol conjugates of doxorubicin: Preparation, *in vitro* efficacy and intracellular distribution. *Bioorg. Med. Chem.* **7,** 2517–2524 (1999).
18. Bae, Y. *et al.* Preparation and biological characterization of polymeric micelle drug carriers with intracellular pH-triggered drug release property: Tumor permeability, controlled subcellular drug distribution, and enhanced *in vivo* antitumor efficacy. *Bioconjug. Chem.* **16,** 122–130 (2005).
19. Dreher, M. R. *et al.* Evaluation of an elastin-like polypeptide–doxorubicin conjugate for cancer therapy. *J. Control. Release* **91,** 31–43 (2003).
20. Lopes de Menezes, D. E. & Mayer, L. D. Pharmacokinetics of Bcl-2 antisense oligonucleotide (G3139) combined with doxorubicin in SCID mice bearing human breast cancer solid tumor xenografts. *Cancer Chemother. Pharmacol.* **49,** 57–68 (2002).
21. Singal, P. K. & Iliskovic, N. Doxorubicin-induced cardiomyopathy. *N. Engl. J. Med.* **339,** 900–905 (1998).
22. Tewey, K. M., Rowe, T. C., Yang, L., Halligan, B. D. & Liu, L. F. Adriamycin-induced DNA damage mediated by mammalian DNA topoisomerase II. *Science* **226,** 466–468 (1984).
23. Nitiss, J. L. Targeting DNA topoisomerase II in cancer chemotherapy. *Nature Rev. Cancer* **9,** 338–350 (2009).
24. Drummond, J. T., Anthoney, A., Brown, R. & Modrich, P. Cisplatin and adriamycin resistance are associated with MutLalpha and mismatch repair deficiency in an ovarian tumor cell line. *J. Biol. Chem.* **271,** 19645–19648 (1996).
25. Hao, X. Y., Bergh, J., Brodin, O., Hellman, U. & Mannervik, B. Acquired resistance to cisplatin and doxorubicin in a small cell lung cancer cell line is correlated to elevated expression of glutathione-linked detoxification enzymes. *Carcinogenesis* **5,** 1167–1173 (1994).
26. Kabanov, A. V. *et al.* Polymer genomics: Shifting the gene and drug delivery paradigms. *J. Control. Release* **101,** 259–271 (2005).
27. Kabanov, A. V. Polymer genomics: An insight into pharmacology and toxicology of nanomedicines. *Adv. Drug Deliv. Rev.* **58,** 1597–1621 (2006).
28. Batrakova, E. V. *et al.* Alteration of genomic responses to doxorubicin and prevention of MDR in breast cancer cells by a polymer excipient: Pluronic P85. *Mol. Pharmaceut.* **3,** 113–123 (2006).
29. Veronese, F. M. *et al.* PEG-doxorubicin conjugates: Influence of polymer structure on drug release, *in vitro* cytotoxicity, biodistribution, and antitumor activity. *Bioconjug. Chem.* **16,** 775–784 (2005).
30. Kwon, G. *et al.* Block copolymer micelles for drug delivery: Loading and release of doxorubicin. *J. Control. Release* **48,** 195–201 (1997).
31. Kataoka, K., Kwon, G. S., Yokoyama, M., Okano, T. & Sakurai, Y. Block-copolymer micelles as vehicles for drug delivery. *J. Control. Release* **24,** 119–132 (1993).
32. Kataoka, K., Harada, A. & Nagasaki, Y. Block copolymer micelles for drug delivery: Design, characterization and biological significance. *Adv. Drug Deliv. Rev.* **47,** 113–131 (2001).
33. Ulbrich, K. *et al.* Polymeric anticancer drugs with pH-controlled activation. *Int. J. Pharmaceut.* **277,** 63–72 (2004).
34. Chytil, P. *et al.* New HPMA copolymer-based drug carriers with covalently bound hydrophobic substituents for solid tumour targeting. *J. Control. Release* **127,** 121–130 (2008).
35. Anton, N., Benoit, J. P. & Saulnier, P. Design and production of nanoparticles formulated from nano-emulsion templates—a review. *J. Control. Release* **128,** 185–199 (2008).
36. Huang, X., Jain, P. K., El-Sayed, I. H. & El-Sayed, M. A. Gold nanoparticles: Interesting optical properties and recent applications in cancer diagnostics and therapy. *Nanomedicine* **2,** 681–693 (2007).
37. Martin, C. R. & Kohli, P. The emerging field of nanotube biotechnology. *Nat. Rev. Drug Discov.* **2,** 29–37 (2003).
38. Nori, A. & Kopecek, J. Intracellular targeting of polymer-bound drugs for cancer chemotherapy. *Adv. Drug Deliv. Rev.* **57,** 609–636 (2005).
39. Kratz, F. *et al.* Development and *in vitro* efficacy of novel MMP2 and MMP9 specific doxorubicin albumin conjugates. *Bioorg. Med. Chem. Lett.* **11,** 2001–2006 (2001).

Acknowledgements

This work was supported with NIH grant 5F32-CA-123,889 to J.A.M. and NIH grant R01-EB-00188 to A.C. We thank M. Dewhirst, M. Zalutsky and M. Dreher for advice regarding experimental design and analysis. We thank F. C. Szoka Jr, for the use of C26 cells and B. Papahadjopoulos-Sternberg for preparation of freeze-fracture electron microscopy images. We thank S. Morales, M. Schneiderman, K. Fitzgerald and K. Liang for expression and purification of CPs used in this study.

Author contributions

J.A.M., M.C. and A.C. designed experiments, analysed data and prepared the manuscript. J.A.M., M.C., J.R.M., W.L. and A.J.S carried out experiments and analysed data.

Additional information

The authors declare competing financial interests: details accompany the full-text HTML version of the paper at www.nature.com/naturematerials. Supplementary information accompanies this paper on www.nature.com/naturematerials. Reprints and permissions information is available online at http://npg.nature.com/reprintsandpermissions. Correspondence and requests for materials should be addressed to A.C.